How to cite: *Angew. Chem. Int. Ed.* **2022,** *61,* e202205413
International Edition: doi.org/10.1002/anie.202205413
German Edition: doi.org/10.1002/ange.202205413

Zeolites

Electron Diffraction Enables the Mapping of Coke in ZSM-5 Micropores Formed during Methanol-to-Hydrocarbons Conversion

Julian T. C. Wennmacher[+], Soheil Mahmoudi[+], Przemyslaw Rzepka, Sung Sik Lee, Tim Gruene, Vladimir Paunović,* and Jeroen A. van Bokhoven**

Abstract: Unveiling the coke formation in zeolites is an essential prerequisite for tackling the deactivation of these catalysts in the transformations of hydrocarbons. Herein, we present the direct mapping of coke in the micropores of ZSM-5 catalysts used in methanol-to-hydrocarbons conversion by single-crystal electron diffraction analysis. The latter technique revealed a polycyclic aromatic structure along the straight channel, wherein the high-quality data permit refinement of its occupancy to about 40 %. These findings were exploited to analyze the evolution of micropore coke during the reaction. Herein, coke-associated signals, which correlate with the activity loss, indicate that the nucleation of coke commences in the intersections of sinusoidal and straight channels, while the formation of coke in the straight pores occurs in the late stages of deactivation. The findings uncover an attractive method for analyzing coke deposition in the micropore domain.

[*] Dr. J. T. C. Wennmacher,[+] Dr. P. Rzepka, Dr. V. Paunović, Prof. Dr. J. A. van Bokhoven
Institute for Chemical and Bioengineering, Department of Chemistry and Applied Biosciences, ETH Zurich
Vladimir-Prelog-Weg 1, 8093 Zurich (Switzerland)
and
Laboratory for Catalysis and Sustainable Chemistry, Paul Scherrer Institute
Forschungsstrasse 111, 5232 Villigen PSI (Switzerland)
E-mail: vladimir.paunovic@chem.ethz.ch
jeroen.vanbokhoven@chem.ethz.ch

S. Mahmoudi,[+] Dr. T. Gruene
Institute of Inorganic Chemistry, Faculty of Chemistry, University of Vienna
Währinger Strasse 42, 1090 Vienna (Austria)
E-mail: tim.gruene@univie.ac.at

S. Mahmoudi[+]
Vienna Doctoral School in Chemistry (DoSChem), University of Vienna
Währinger Strasse 42, 1090 Vienna (Austria)

Dr. S. Sik Lee
Scientific Center of Optical and Electron Microscopy, ETH Zurich
Otto-Stern-Weg 3, 8093 Zurich (Switzerland)

[+] These authors contributed equally to this work.

Zeolites are essential catalysts in the processing of carbon-based raw materials into valued chemicals and liquid fuels.[1] A prototypical example of such process is methanol-to-hydrocarbons (MTH) conversion, which enables the production of the world's most-needed alkenes, gasolines, and aromatics from a range of fossil and renewable alternatives to crude oil feedstock.[1,2] The MTH coupling, which proceeds via a complex dual-cycle hydrocarbon pool mechanism, is commercially performed over ZSM-5 and SAPO-34 catalysts.[2] However, like other zeolite-catalyzed transformations of hydrocarbons, the MTH reaction is substantially limited by the accumulation of the so-called coke species in the zeolite micropores (internal coke) and at its outer surface (external coke). Coke occludes the active sites and hampers the molecular diffusion, eventually causing activity loss.[2,3] This introduces the need for the recurrent regeneration via coke combustion at elevated temperatures ($>$823 K), which wastes a fraction of methanol feed converted to coke and provokes the zeolite degradation.[2a,4]

Consequently, minimizing zeolite coking is one of the long-standing objectives that has spurred intense research on the nature of coke and the mechanism of its formation.[3,5] Numerous mass spectrometry, spectroscopic, and theoretical studies identified alkylated polycyclic aromatic hydrocarbons (PAH) and graphite-like molecules as the principal components of internal and external coke, respectively.[3,6] The composition of coke and the rate of its formation are strongly dependent on framework topology, crystallite size, nature, and density of the acid sites.[7] As a result, the subtle differences in pore geometries, acid-site densities, and diffusion lengths across the catalyst particles cause the variable propensity of coke to deposit in different sections of the micropores.[3a,5b,8,9] Pinpointing coke in the micropores is therefore of vital interest for in-depth understanding of the coking mechanism. Currently available methods, like X-ray diffraction and imaging techniques, do not provide a sufficient resolution to localize the micropore coke in practically relevant zeolite crystals as their size is typically less than a few microns.[6a,8a,9] The present insights into the micropore coking are therefore derived from theory and indirect observation of coke location in model crystals.[6a–c,8b] Herein, theoretical calculations predict that coke precursors are formed in the intersections of the straight and sinusoidal channels, and that linear PAH are preferably located along the straight pores.[6b] The polarization-dependent UV/Vis diffuse reflectance spectroscopy of the uniformly-oriented ZSM-5 indicated that straight

channels are mostly occluded by the linear PAH that compose internal coke, while the external coke is preferentially formed at the openings of the sinusoidal channels.[6c] This provided a hint that coking is likely initiated in the channel intersections and that PAH are formed along the straight channels. Still, the analysis by the electron energy loss spectroscopy and electron microscopy suggested that external coke is preferentially deposited at the outlets of straight pores of ZSM-5 crystals with short *b*-axis, while it evenly covers the openings of both channel types in the crystals with longer *b*-axis.[8b] These results imply that altered diffusion lengths in model materials can cause different coking behavior in comparison to the realistic zeolites. Hence, the confirmation of the micropore coking mechanism would benefit from a direct 3D mapping of coke in the micropores of zeolites of industrial relevance.

Herein, we present a novel approach to discern the deposition of coke in the micropores during the MTH reaction, which is based on single-crystal electron diffraction (ED). In comparison to the more commonly applied powder X-ray diffraction (PXRD), the ED enables ab-initio structure determination from zeolites at sub-micrometer dimensions, which are relevant for catalysis.[10] In addition, the electrons interaction with mater makes the signal of light atoms such as carbon that are located near the heavier atoms such as silicon and aluminum to be better resolved than with X-ray diffraction. The latter difference is particularly relevant for analyzing partially disordered atoms of coke, since the disorder lowers the scattering power of the lighter atoms. Still, although used to pinpoint the framework atoms of zeolites and simple molecules adsorbed inside them, the applicability of ED to allocate the complex and more disordered structures such as PAH in the micropores has not been demonstrated.[10b–d]

Aiming to unveil the potential of ED to localize the coke, we commenced our study by examining the commercial ZSM-5 zeolite with a Si:Al ratio of 37 after its deactivation in the MTH reaction. This parent material, which is denoted as Z_{0h}, is one of the most frequently studied MTH catalysts and was therefore selected as an exemplary case. Its particle size range (ca. 0.2–1 μm), textural, crystallographic, and acid properties are consistent with earlier reports (Table 1, Figure S1 in the Supporting Information).[7b,c] The MTH reaction over Z_{0h} was performed at increased temperature (773 K) and methanol concentration (49 mol %), and reduced weight hourly space velocity ($16\,g_{CH_3OH}\,g_{cat}^{-1}\,h^{-1}$), which led to a complete initial conversion and fast deactivation (Figure S2). The resulting deactivated sample, which is denoted as Z_c, exhibited a high coke content (ca. 19.2 wt %) and prominent decrease of the micropore volume (from 0.12 to 0.04 $cm^3\,g^{-1}$, Table 1). In addition, the surface of Z_c was enriched with carbon, pointing to the formation of external coke (Table 1, Figure S2). PXRD analysis of Z_c indicated a much smaller difference between *a* and *b* unit cell parameters (0.078 Å) in comparison to the Z_{0h} sample (0.184 Å, Table 1). This implies an increased lattice microstrain that is induced by high content of internal coke,[5c] which made Z_c sample highly suitable for evaluating the potential of ED to pinpoint coke. About 50 particles were analysed at 84 K (Figure S3). Thereafter, datasets of 10 selected crystals were merged to enhance data completeness and statistics (Tables S1, S6). Strikingly, Z_c catalyst displayed a very intense signal in the zones of crystals corresponding to the micropores, which is clearly differentiated from the background noise (Figure 1a, Figure S4). The signal peaks take a planar arrangement along the straight channels (Figure 1b,c). Notably, the peaks clearly belong to a short PAH fragment of 11 carbon atoms (Figure 1d, Figure S5). The fragment does not strictly follow the 2_1 symmetry, leading to slight distortion from expected bond lengths and angles, and a reduction of the crystallographic occupancy to ca. 40 % (Figure S6). The symmetry element completes this fragment to a linear PAH along the straight channel with a 6-ring protruding into the sinusoidal channel. Besides, some peaks were also observable in the sinusoidal channels. Although they could not be modeled to a specific structure, their distances of ca. 1.5 Å closely match the typical C–O and C–C bond lengths in methanol and saturated aliphatics. Thus, the ED analysis of Z_c sample reveals that PAH molecules attain a high degree of ordering at increased extent of coke accumulation in the pores. This can be rationalized by a decreased motion flexibility due to increased ring condensation and reduced free micropore volume. Most of the coke-associated ED signal is located in the channel intersections (Figure 1a). This is well-aligned with the previous spectroscopic and theoretical studies, which identified this most spacious void region as the most susceptible to PAH evolution.[6b,c] Moreover, the fraction of the signal in the straight (ca. 29 %) is much higher than in the sinusoidal (ca. 16 %) pores (Figure 1a). This corrobo-

Table 1: Textural, compositional, and crystallographic properties of ZSM-5 catalysts in fresh form and after deactivation in MTH reaction.

Catalyst	V_{micro}[a]/ [$cm^3\,g^{-1}$]	S_{micro}[a]/ [$cm^2\,g^{-1}$]	S_{BET}[b]/ [$cm^2\,g^{-1}$]	C_{coke}[c]/ [wt %]	C:Si_{bulk}[c]/ [mol mol^{-1}]	C:$Si_{surface}$[d]/ [mol mol^{-1}]	Lattice parameters[e] [Å]			
							A	*b*	*c*	*a-b*
Z_{0h}	0.120	293	435	0	< 0.01	0.14	20.096	19.912	13.398	0.184
Z_c	0.04	110	113	19.2	1.13	4.1	20.078	20.000	13.434	0.078
Z_{1h}	0.115	274	409	3.0	0.15	0.17	20.106	19.929	13.408	0.177
Z_{5h}	0.105	249	373	4.0	0.20	0.21	20.112	19.939	13.414	0.173
Z_{12h}	0.085	201	282	8.2	0.43	0.30	20.099	19.949	13.419	0.150
$Z_{19.5h}$	0.07	172	233	10.2	0.54	0.49	20.087	19.968	13.429	0.119

Determined by: [a] t-plot and [b] BET methods, [c] TGA, [d] XPS, [e] PXRD and Pawley method.

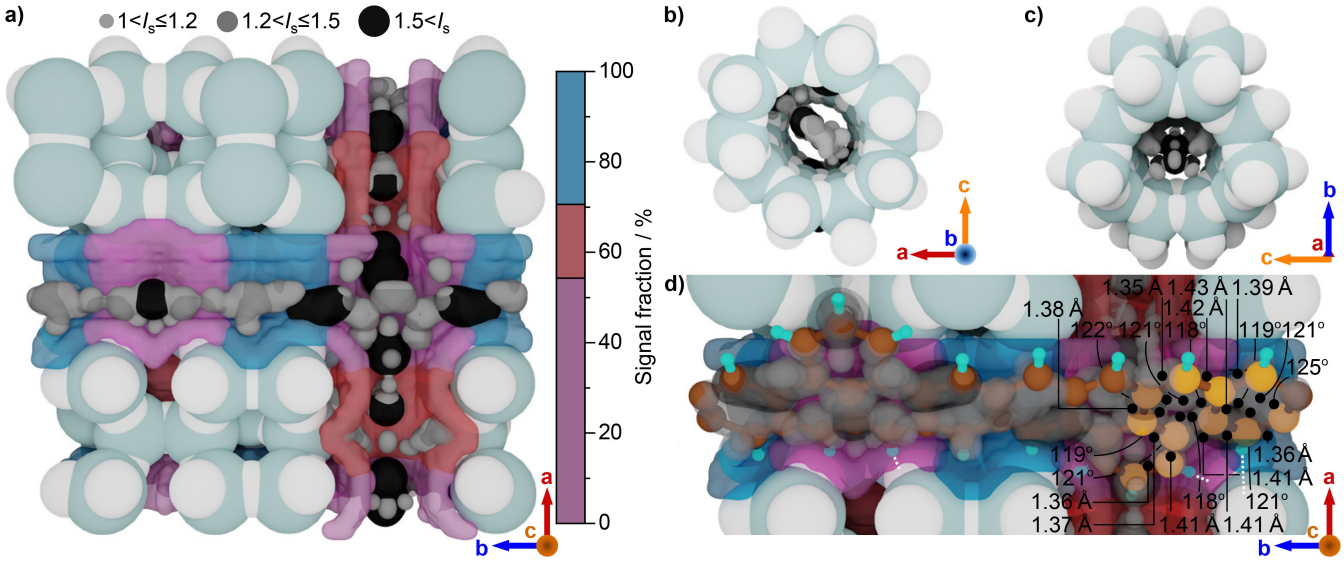

Figure 1. a) Distribution of coke-associated signal in the zeolite unit cell as extracted from the direct electron diffraction maps of severely-coked Z_c catalyst. Views along the b) straight and c) sinusoidal channels. d) The most intense coke-associated signals that protrude through the straight channel can be modelled as a molecule comprising three fused aromatic rings, with indicated bond lengths and angles. The crystallographically equivalent carbon and hydrogen atoms are colored in light orange and turquoise, respectively. Dashed lines indicate the possible hydrogen bonds. The tetrahedral (Al or Si) and oxygen framework sites are colored in green and white, respectively. Crystal orientation is indicated with respective coordinates. The straight and sinusoidal channels and their intersections are indicated with blue, red, and pink isosurfaces, respectively. The standardized signals for which $I_s > 1$ were considered as coke-associated, and their intensity is indicated with a map shown above the panel a), which also applies to b) and c). The fraction of signals in different micropore sections is presented with a bar plot in a), in which the color code corresponds to the channel designations by isosurfaces.

rates the assumption that deactivation is primarily caused by the coke formation in the straight channels.

Intrigued by the observation of the coke-associated signal, we further evaluated the applicability of ED to map the evolution of micropore coke during catalyst deactivation in MTH conversion. For this purpose, the MTH reaction over Z_{0h} was performed at sub-complete conversion, which ensures that catalyst bed experiences the coking contributions of methanol and products and minimizes the coke gradients along the reactor (Figure S7). The reaction was quenched after 1, 5, 12 and 19.5 h, and the properties of coke in thus obtained partially deactivated Z_{1h}, Z_{5h}, Z_{12h}, and $Z_{19.5h}$ samples were examined. In line with the increased deactivation, the coke content increased in the order Z_{1h} (3.0 wt %) < Z_{5h} (4.0 wt %) < Z_{12h} (8.2 wt %) < $Z_{19.5h}$ (10.2 wt %), which is paralleled by a reduction of the micropore volume (from 0.12 to 0.07 $cm^3 g^{-1}$) and BET surface area (from 435 to 233 $m^2 g^{-1}$, Table 1). Consistent with previous studies, ^{13}C cross-polarization magic angle spinning NMR and Raman spectroscopies demonstrated that with increasing coke content in Z_{1h}-$Z_{19.5h}$ catalysts, the fraction of more condensed and less-alkylated PAH also increased (Figure S7).[6d] The confocal fluorescence microscopy showed uniform distribution of the mono-, bi-, tri-, and tetracyclic arenes across the particles in all the samples (Figure S7).[6a] The surface C:Si ratio increased from 0.17 to 0.49 mol mol^{-1}, which does not deviate substantially from the change of the bulk carbon content, pointing to the absence of extensive surface coking (Table 1, Figure S8). PXRD data evidenced a contraction of the crystal along the *a* and the elongation along the *b* axis with deactivation, which points to the increasing content of internal coke (Table 1, Figure S9).[5c]

To gain insights into the coking at the micropore level, individual crystals of Z_{1h}-$Z_{19.5h}$ catalysts were investigated by ED (Figure 2, Figures S10, S11, Tables S2–S6). In agreement with the PXRD results, the ED data of coked ZSM-5 zeolites indicated the equalization of the *a* and *b* unit cell parameters (Table S6). Notably, both the direct and the difference ED maps showed a guest signal in the micropores (Figure 2, Figures S10, S11). Considering a much bigger size of a crystal with respect to a unit cell, the coke-associated signal is mostly reflecting coke in the micropores in the crystal bulk. This signal was particularly strong in the channel intersections, wherein its intensity increased in the order Z_{1h} (54 a.u.) < Z_{5h} (135 a.u.) < Z_{12h} (170 a.u.) < $Z_{19.5h}$ (213 a.u.), and was lower than in severely coked Z_c catalyst. Similar to Z_c, the most intense peaks of $Z_{19.5h}$ sample exhibited a planar arrangement, which resembles to the carbon atoms in an aromatic molecule with a hybridized sp^2 system (Figure S12). The observation of the maximum signal density in the channel intersections is well-aligned with the proposal that this most spacious void space of the ZSM-5 crystal is the main region in which the aromatic chain carriers reside during the MTH reaction.[2,6b,c] With the increasing extent of coking, the coke-associated signal in the sinusoidal channels moderately increased, while the signal fraction in the straight channels increased from Z_{1h} (ca. 0 %) to Z_{12h} (ca. 9 %) and $Z_{19.5h}$ (ca. 8 %, Figure 2). Along with a high fraction of the signal in the straight channels of the Z_c

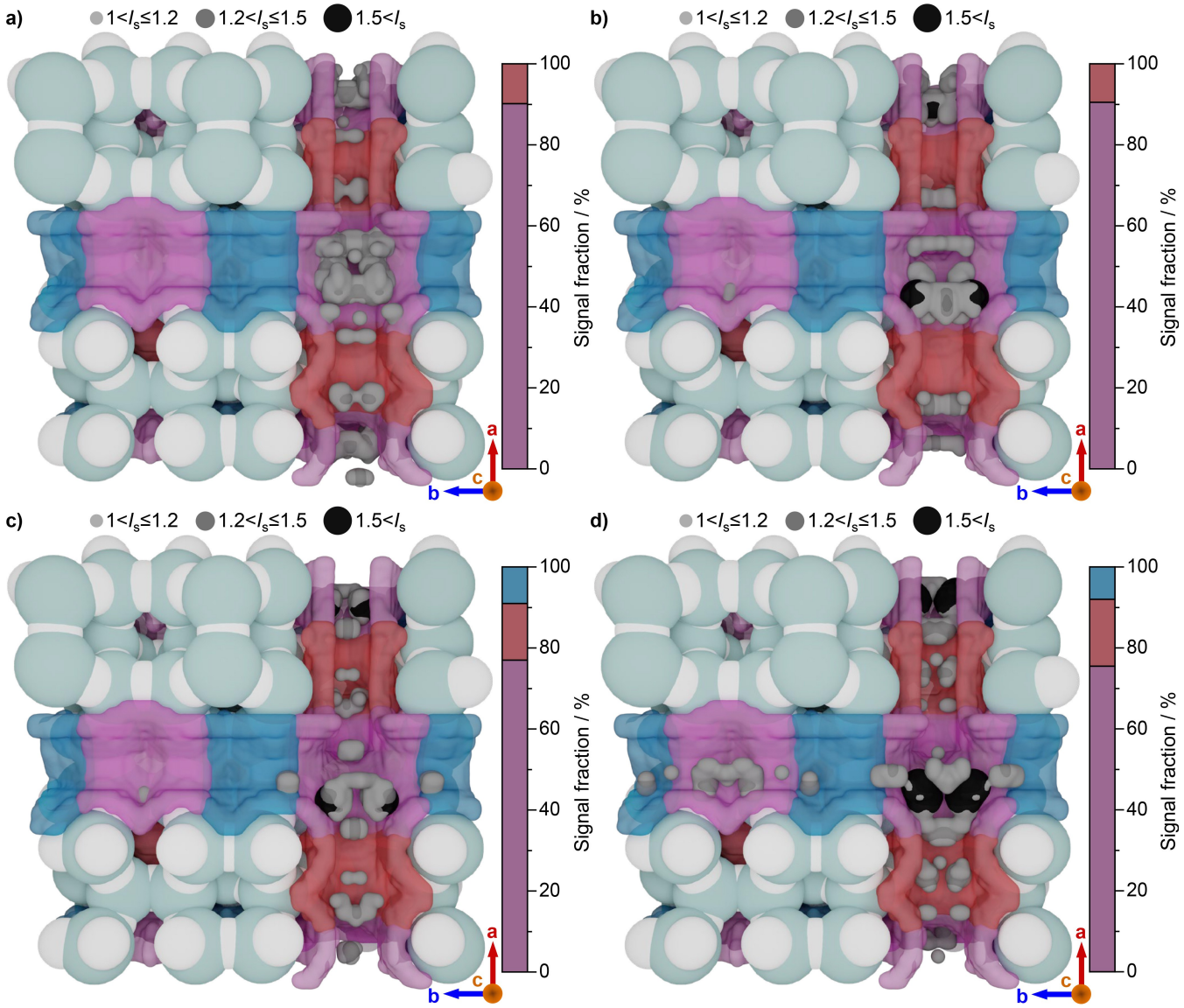

Figure 2. Distribution of the standardized coke-associated signal in the zeolite unit cell as extracted from the direct electron diffraction maps in a) Z_{1h}, b) Z_{5h}, c) Z_{12h} and d) $Z_{19.5h}$ catalysts. Framework atoms, micropore sections, signal intensities, and distribution are designated as detailed in the caption of Figure 1.

material, these results demonstrate that after the nucleation of coke in the channel intersections of the ZSM-5, the nucleation centers are progressively condensed through the straight micropores. This parallels the increasing content of the heavier aromatics in coke that may be linked to the condensation of the aromatic rings along the latter channels (Figure S7). A low fraction of the coke-associated signal in the straight pores of the most deactivated catalysts suggests that coke formation in this microporous region has a high impact on the catalyst deactivation. The coke growth observed by ED is consistent with the previous reports indicating that the formation of PAH (bi-and tri-cyclic) in ZSM-5 is more favored in the straight channels, due to lower geometrical constrains affecting their planar configuration.[6b,c] Such coking mechanism inferred from ED analysis provides a hint that suppression of coke condensation along the straight channels can be a strategy to enhance the catalyst life-time.

In summary, we demonstrated that ED is a powerful tool to pinpoint the location and 3D structure of coke in zeolite micropores. It enabled to disclose information of weak next to heavy scattering centers, and to retain more signal of disordered molecules, while preserving the sample structure. ED can detect the presence of small amounts of coke in the micropores (ca. $\geq$1 wt %). At higher coke loadings (ca. $\geq$10 wt %), crystallographic ordering of PAH increases, which along with stronger signal permits their structural refinement. The results provide experimental evidence that coke formation starts in the channel intersections. The loading of the straight pores with coke coincides with increasing degree of coke condensation and a high activity loss in the late stages of deactivation. These

findings open up new perspectives for comprehending the mechanism of micropore coking.

Acknowledgements

The authors acknowledge Dr. Vitaly Sushkevich from PSI Villigen for pyridine FTIR analysis, Dr. René Verel from ETH Zurich for the support in performing MAS NMR analysis, Dr. Roland Hauert from EMPA Dübendorf for XPS measurements, ScopeM for the access to the Raman instrument, PSI Detector Group for the JUNGFRAU detector and support. JCTW was supported by the by the Swiss National Science Foundation (Project No. 200021_169258). The Energy System Integration platform of the Paul Scherrer Institute is acknowledged for financial support. Open access funding provided by Eidgenössische Technische Hochschule Zürich.

Conflict of Interest

The authors declare no conflict of interest.

Data Availability Statement

The crystallographic data are available free of charge from the Cambridge Crystallographic Data Centre under the following CCDC numbers: 2153995 (Z_c), 2125197 (Z_{1h}), 2125198 (Z_{5h}), 2125198 (Z_{5h}), 2125199 (Z_{12h}), and 2125200 ($Z_{19.5h}$). Other data that support the findings of this study are available from the corresponding author upon reasonable request.

Keywords: Catalysis · Coke Characterization · Deactivation · Electron Diffraction · Microporous Materials

[1] J. Čejka, A. Corma, S. Zones, *Zeolites and Catalysis: Synthesis, Reactions and Applications*, Wiley-VCH, Weinheim, **2010**.

[2] a) U. Olsbye, S. Svelle, M. Bjrgen, P. Beato, T. V. W. Janssens, F. Joensen, S. Bordiga, K. P. Lillerud, *Angew. Chem. Int. Ed.* **2012**, *51*, 5810–5831; *Angew. Chem.* **2012**, *124*, 5910–5933; b) I. Yarulina, A. D. Chowdhury, F. Meirer, B. M. Weckhuysen, J. Gascon, *Nat. Catal.* **2018**, *1*, 398–411.

[3] a) S. Müller, Y. Liu, M. Vishnuvarthan, X. Sun, A. C. Van Veen, G. L. Haller, M. Sanchez-Sanchez, J. A. Lercher, *J. Catal.* **2015**, *325*, 48–59; b) N. Wang, Y. Zhi, Y. Wei, W. Zhang, Z. Liu, J. Huang, T. Sun, S. Xu, S. Lin, Y. He, A. Zheng, Z. Liu, *Nat. Commun.* **2020**, *11*, 1079.

[4] F. Schmidt, C. Hoffmann, F. Giordanino, S. Bordiga, P. Simon, W. Carrillo-Cabrera, S. Kaskel, *J. Catal.* **2013**, *307*, 238–245.

[5] a) A. G. Alvarez, H. Viturro, R. D. Bonetto, *Mater. Chem. Phys.* **1992**, *32*, 135–140; b) J. E. Schmidt, J. D. Poplawsky, B. Mazumder, Ö. Attila, D. Fu, D. A. M. de Winter, F. Meirer, S. R. Bare, B. M. Weckhuysen, *Angew. Chem. Int. Ed.* **2016**, *55*, 11173–11177; *Angew. Chem.* **2016**, *128*, 11339–11343; c) D. Rojo-Gama, M. Nielsen, D. S. Wragg, M. Dyballa, J. Holzinger, H. Falsig, L. F. Lundegaard, P. Beato, R. Y. Brogaard, K. P. Lillerud, U. Olsbye, S. Svelle, *ACS Catal.* **2017**, *7*, 8235–8246; d) Y. Shen, T. T. Le, D. Fu, J. E. Schmidt, M. Filez, B. M. Weckhuysen, J. D. Rimer, *ACS Catal.* **2018**, *8*, 11042–11053.

[6] a) D. Mores, E. Stavitski, M. H. F. Kox, J. Kornatowski, U. Olsbye, B. M. Weckhuysen, *Chem. Eur. J.* **2008**, *14*, 11320–11327; b) R. Y. Brogaard, B. M. Weckhuysen, J. K. Nørskov, *J. Catal.* **2013**, *300*, 235–241; c) D. Fu, O. van der Heijden, K. Stanciakova, J. E. Schmidt, B. M. Weckhuysen, *Angew. Chem. Int. Ed.* **2020**, *59*, 15502–15506; *Angew. Chem.* **2020**, *132*, 15632–15636; d) P. Ferri, C. Li, C. Paris, A. Vidal-Moya, M. Moliner, M. Boronat, A. Corma, *ACS Catal.* **2019**, *9*, 11542–11551.

[7] a) T. Liang, J. Chen, Z. Qin, J. Li, P. Wang, S. Wang, G. Wang, M. Dong, W. Fan, J. Wang, *ACS Catal.* **2016**, *6*, 7311–7325; b) I. Yarulina, K. De Wispelaere, S. Bailleul, J. Goetze, M. Radersma, E. Abou-Hamad, I. Vollmer, M. Goesten, B. Mezari, E. J. M. Hensen, J. S. Martínez-Espín, M. Morten, S. Mitchell, J. Perez-Ramirez, U. Olsbye, B. M. Weckhuysen, V. Van Speybroeck, F. Kapteijn, J. Gascon, *Nat. Chem.* **2018**, *10*, 804–812; c) M. Choi, K. Na, J. Kim, Y. Sakamoto, O. Terasaki, R. Ryoo, *Nature* **2009**, *461*, 246–249; d) X. Zhang, D. Liu, D. Xu, S. Asahina, K. A. Cychosz, K. V. Agrawal, Y. Al Wahedi, A. Bhan, S. Al Hashimi, O. Terasaki, M. Thommes, M. Tsapatsis, *Science* **2012**, *336*, 1684–1687.

[8] a) K. De Wispelaere, C. S. Wondergem, B. Ensing, K. Hemelsoet, E. J. Meijer, B. M. Weckhuysen, V. Van Speybroeck, J. Ruiz-Martínez, *ACS Catal.* **2016**, *6*, 1991–2002; b) N. Wang, W. Sun, Y. Hou, B. Ge, L. Hu, J. Nie, W. Qian, F. Wei, *J. Catal.* **2018**, *360*, 89–96.

[9] M. Veselý, R. Valadian, L. Merten Lohse, M. Toepperwien, K. Spiers, J. Garrevoet, E. T. C. Vogt, T. Salditt, B. M. Weckhuysen, F. Meirer, *ChemCatChem* **2021**, *13*, 2494–2507.

[10] a) B. K. Vainshtein, *Q. Rev. Chem. Soc.* **1960**, *14*, 105–132; b) M. Gemmi, E. Mugnaioli, T. E. Gorelik, U. Kolb, L. Palatinus, P. Boullay, S. Hovmöller, J. P. Abrahams, *ACS Cent. Sci.* **2019**, *5*, 1315–1329; c) M. Debost, P. B. Klar, N. Barrier, E. B. Clatworthy, J. Grand, F. Laine, P. Brázda, L. Palatinus, N. Nesterenko, P. Boullay, S. Mintova, *Angew. Chem. Int. Ed.* **2020**, *59*, 23491–23495; *Angew. Chem.* **2020**, *132*, 23697–23701; d) T. Grüne, J. J. Holstein, G. H. Clever, B. Keppler, *Nat. Chem. Rev.* **2021**, *5*, 660–668; e) M. Ge, Y. Wang, F. Carraro, W. Liang, M. Roostaeinia, S. Siahrostami, D. M. Proserpio, C. Doonan, P. Falcaro, H. Zheng, X. Zou, Z. Huang, *Angew. Chem. Int. Ed.* **2021**, *60*, 11391–11397; *Angew. Chem.* **2021**, *133*, 11492–11498.

Manuscript received: April 12, 2022
Accepted manuscript online: May 5, 2022
Version of record online: May 25, 2022